Surface Measurements of Precipitation from an Ocean Mooring: The Underwater Acoustic Log from the South China Sea*

JEFFREY A. NYSTUEN

Applied Physics Laboratory, University of Washington, Seattle, Washington

MICHAEL J. MCPHADEN AND H. PAUL FREITAG

Pacific Marine Environmental Laboratory, National Oceanic and Atmospheric Administration, Seattle, Washington

(Manuscript received 29 September 1999, in final form 19 April 2000)

ABSTRACT

Surface measurements of precipitation in oceanic environments have proven especially difficult to obtain because traditional technologies such as tipping-bucket rain gauges are unsuitable for deployment from oceanic platforms such as ships and moorings. Recently, the Pacific Marine Environmental Laboratory of the National Oceanic and Atmospheric Administration has modified a collection gauge, the R. M. Young Company rain gauge, for long-term deployment on deep ocean moorings. This instrumentation package was deployed during part of the South China Sea Monsoon Experiment. Also deployed on the same mooring were two acoustic rain gauges (ARGs) that monitor precipitation through the interpretation of the high-frequency, from 500 to 50 000 Hz, underwater sound field. The mooring was located at 20°22.2′N, 116°31.2′E and was in place from 7 April–5 June 1998. Unfortunately, pirates stole the surface instrumentation on 6 May 1998, limiting data from the R. M. Young rain gauge to satellite transmissions prior to the attack. The ARGs survived the attack and reported data throughout the deployment. The acoustic data are interpreted to provide quantification of wind speed; detection, classification, and quantification of rainfall; and the detection and quantification of near-surface bubble layers. Percentage-of-time-raining data from the two rainfall measurements are in excellent agreement. Based on comparison with the R. M. Young rain gauge data, modified acoustic rainfall algorithms are proposed. The acoustic detection of several instances of high near-surface bubble injections during extremely heavy rainfall is described.

1. Introduction

Global measurements of the distribution of precipitation are recognized as a particularly important problem for climatologists. Many satellite methods for rainfall measurement have been proposed (Ebert et al. 1996). The lack of surface rainfall data is a recognized problem, especially over the oceans (Barrett et al. 1995). To help to address this problem, a dedicated satellite, the Tropical Rainfall Measuring Mission (TRMM), has been launched. As part of the TRMM program, the National Aeronautics and Space Administration (NASA) has an extensive ground validation program that includes the most recent advances in rainfall measurement technologies.

During 1998, a major international field experiment, the South China Sea Monsoon Experiment (SCSMEX) took place. The goal of SCSMEX was to understand better the key physical processes for the onset, maintenance, and variability of the monsoon over Southeast Asia and southern China (Lau 1998). Precipitation observations were a principal part of this experiment and included a dual-Doppler radar array, land-based rain gauges, and an autonomous temperature line acquisition system (ATLAS) ocean mooring near Dongsha Island (20°N, 116°E) in the northern part of the South China Sea (Fig. 1). Data from the ATLAS mooring are the focus of this paper. A new instrumentation package has been designed for the ATLAS moorings package (Milburn et al. 1996), including an R. M. Young Company precipitation sensor modified for long-term deployments. Also mounted on this mooring were two acoustic rain gauges (ARGs) at 20- and 22-m depth below the surface.

In situ measurements of air–sea exchange processes are often difficult to obtain because of the difficulty of maintaining instruments at the ocean surface. Several important processes contributing to the heat, momen-

* Pacific Marine Environment Laboratory Contribution No. 2179.

Corresponding author address: Jeffrey A. Nystuen, Senior Oceanographer, Applied Physics Laboratory, University of Washington, 1013 NE 40th St., Seattle, WA 98105-6698.
E-mail: nystuen@apl.washington.edu

tum, water, and gas exchange across the ocean–atmosphere interface, including wave breaking, precipitation, and the generation of near-surface bubbles, generate and modify the underwater sound in the frequency range from 500 to 50 000 Hz. This fact has been known for a long time (Knudsen et al. 1948; Wenz 1962), and has led to attempts to quantify these processes using the underwater ambient sound field (Shaw et al. 1978; Evans et al. 1984; Lemon et al. 1984; Vagle et al. 1990; Nystuen et al. 1993; Nystuen 1996). The acoustic data from these ARGs are interpreted to provide quantitative measurements of wind speed; detection, classification and quantification of rainfall; and the detection of near-surface bubble layers. This experiment is one of the first efforts to make acoustically based geophysical measurements from an ocean surface mooring.

Two intensive observation periods (IOPs) from 5 to 25 May and 4 to 23 June 1998 occurred during which, based on the ship's scientific log, a variety of convective systems ranging from frontal stratiform deck to tropical deep convection were observed. Unfortunately the ATLAS mooring suffered vandalism from a pirate attack on or about 6 May. The surface instrumentation was stolen, including the R. M. Young rain gauge, limiting data from this instrument to times prior to the attack. The ARGs, located 20 m below the surface, were not detected by the pirates and continued to function for the duration of the mooring deployment. The mooring was recovered on 6 June, at the start of the second IOP, limiting the acoustic data to 7 April–6 June.

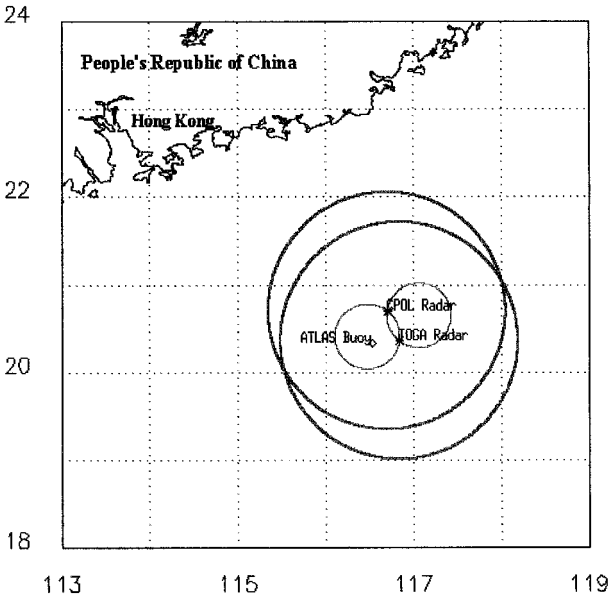

FIG. 1. Map showing the location of the ATLAS mooring and the dual-Doppler radars during SCSMEX. The large circles indicate the limit (150-km range) of full-volume reflectivity measurements from each of the two radars. The inner circles outline the regions where dual-Doppler velocity retrieval is possible. The ATLAS buoy lies within the southwest Doppler lobe.

2. Data description

a. R. M. Young precipitation gauge data

One dataset used in this study comes from an R. M. Young precipitation gauge mounted on a next-generation ATLAS mooring. The ATLAS mooring was developed at the National Oceanic and Atmospheric Administration's (NOAA) Pacific Marine Environmental Laboratory (PMEL; Milburn et al. 1996) and is used extensively across the Pacific basin as part of the Tropical Atmosphere–Ocean (TAO) array (McPhaden et al. 1998). Standard ATLAS measurements include surface winds, air temperature, relative humidity, sea surface temperature, and subsurface temperature to 500-m depths. The next-generation ATLAS is modular in design and allows for additional measurements of rain rate, insolation, and ocean conductivity. The mooring deployed in SCSMEX had all of these sensors except subsurface temperature and conductivity. It was anchored at a depth of about 744 m.

ATLAS data are internally recorded and transmitted to shore in real-time via Service Argos, Inc. To conserve power, the ATLAS only transmits in two 4-h windows chosen to coincide with satellite overpasses during the day. Internally recorded data consist of 10-min samples of all variables except rain accumulation and insolation, which are recorded at 1- and 2-min intervals, respectively. Real-time transmissions consist of daily means and, for insolation and rainfall, additional daily statistics. Transmitted statistics for rainfall are daily mean rain rate, rain-rate standard deviation, and percentage of time raining during the day based on the 1-min samples. For the standard surface meteorological data, the ATLAS buoy also transmits spot samples at the top of the hour (minute 00). The number of Argos satellite overpasses per day in the Tropics (6–8) and the limited period of data transmission typically limit the number of spot hourly samples to about three per day.

Precipitation measurements on next-generation ATLAS moorings are made using R. M. Young Model 50202 precipitation gauges that have been modified by PMEL for integration into the ATLAS electronics. The sensors are mounted at approximately 3 m above mean sea level on the buoy tower. These sensors have a 100-cm^2 catchment cylinder mounted atop a funnel that leads water into a cylindrical measuring tube. Water height within the tube is determined by measuring capacitance. The measuring tube has a storage capacity of 500 ml, after which it automatically drains via a siphon. The relative geometry of the catchment and measuring portions of the sensor result in a total accumulation of 50 mm of rainfall between siphon events. Siphon events take about 30 s and are typically identified by sharp declines in volume for two consecutive samples. In real-time processing, these events are ignored.

The R. M. Young gauge reports a water level within its collection chamber each minute and calculates the

difference to obtain a rainfall rate for that minute. The sensor accuracy is specified by the manufacturer as 1 mm, although maximum calibration residuals are typically less than 5 ml (0.5 mm). Daily mean and standard deviation of rain rate (mm h^{-1}) and percent of time raining are computed from the 1-min rainfall-rate data. Rain-rate resolution for real-time daily means is 0.08 mm h^{-1}. Inspection of 1-min rain data from recovered moorings of the TAO array indicates that instrumental noise levels are generally low, a few tenths of millimeters per hour, relative to the signals of interest. However, there are unexplained episodes of enhanced noise in some sensors. Onboard real-time processing employs a threshold rate of 1 mm h^{-1}, equating all lesser rate values to zero. If significant noise occurs during times of no rain with amplitudes larger than this threshold, it can bias daily statistics to indicate more rain than actually occurred. Fortunately, this type of noise occurs infrequently.

Other sources of noise include undercatch of rainfall in high winds, excessive buoy motion, sea spray, and evaporation from the cylinder. These errors are extremely difficult to quantify. However, for the environmental conditions encountered in the South China Sea during our experiment, these sources of error are not likely to affect the analysis adversely. The R. M. Young precipitation gauge has been used under similar circumstances during the Tropical Ocean and Global Atmosphere Coupled Ocean–Atmosphere Response Experiment (TOGA COARE) on moored and drifting buoys for quantitative analyses of the surface layer salt balance (Anderson et al. 1996; Godfrey et al. 1999). From these and other studies, one might expect *O*(10%) errors in rain rates as measured from the ATLAS buoy.

Because the instrument package was stolen (unbolted from the surface float) on 6 May, the only data available from the surface instruments are the Argos transmissions prior to 6 May. Two groups of data were useful for comparison to the acoustic data. First were the spot hourly values of wind speed, a 2-min average from the most recent hour (minute 00) preceding the satellite overpass. A total of 36 data points were obtained before the mooring was vandalized. The second set of data were the daily summary data from the R. M. Young rain gauge. These data included the average rainfall rate during the preceding 24-h period and the percentage of time that rainfall was recorded during that time period. The rainfall statistics were not available every day because of missed satellite broadcasts. Nonzero values were available on 8 days prior to the pirate attack.

b. The acoustic data

The ARGs consist of an International Transducer Corporation Model ITC-1032 hydrophone, signal preamplifiers, and a recording computer (Onset Computer Corporation Tattletale Model 8). The nominal sensitivity of these instruments is -197 dB relative to 1 V μPa^{-1}, and the equivalent oceanic background noise level of the preamplifier system is about 37 dB relative to 1 μPa^2 Hz^{-1}. Bandpass filters are present to reduce saturation from low-frequency sound (high pass at 2000 Hz) and aliasing from above 50 kHz (low pass at 40 kHz). The ITC-1032 hydrophone sensitivity also rolls off above its resonance frequency, about 40 kHz. The recorded data have been corrected for this frequency sensitivity.

TABLE 1. Frequency bins for the ARGs.

Frequency	ARG-B434 (bin No.)	ARG-A18 (bin No.)
500	1	1
1500	2	2
2400	3	3
3400	4	4
4400	Noise	5
5400	5	6
6300	6	7
7300	7	8
8300	Noise	9
9300	8	10
10 300	9	11
11 200	10	12
12 200	Noise	Noise
13 200	11	13
14 200	12	14
15 100	13	15
16 100	14	16
17 100	Noise	17
18 100	15	18
19 100	16	19
21 000	17	20
22 900	18	21
24 900	19	Noise
26 900	20	22
28 800	21	23
30 800	22	24
32 700	23	25
34 700	24	26
36 600	25	27
38 600	Noise	Noise
40 500	26	28
42 500	27	29
44 400	28	30
46 400	29	31
48 300	30	32
50 300	Noise	Noise

A data collection sequence consisted of four 1024-point time series collected at 100 kHz (10.24 ms each) separated by 5 s. Each time series was fast Fourier transformed to obtain a 512-point (0–50 kHz) power spectrum. These four spectra were averaged together and spectrally compressed to 36 frequency bins, with frequency resolution of 1 kHz from 1 to 20 kHz and 2 kHz from 20 to 50 kHz. The centers of each frequency bin are shown in Table 1. Instrument noise from the Tattletale-8 was present in the data but was confined to a few frequency bins. This noise was identified for each ARG in the time period just prior to deployment (Fig. 2). The contaminated frequency bins for each ARG are shown in Table 1. Data from these frequency bins were not included in subsequent analyses.

Part of the acoustic analysis is the identification of

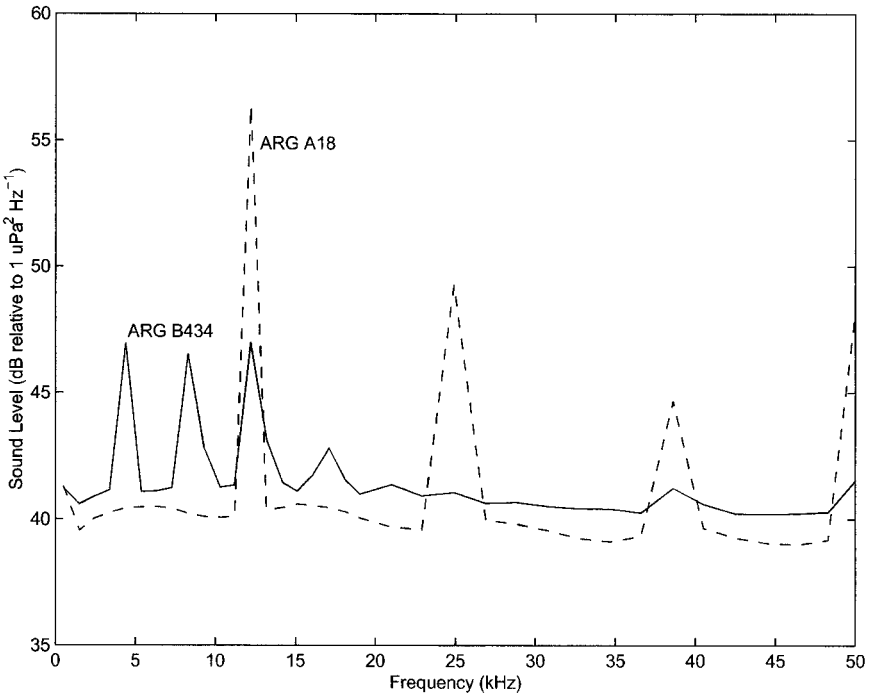

FIG. 2. Instrument noise for the ARGs. The solid line is the ARG-A18 and the dashed line is the ARG-B434. The instrument noise is presented as equivalent acoustic background noise level.

geophysically generated sound from anthropogenic sound (ships, the mooring itself, and the mooring float). It was expected that there would be noise generated by the nearby surface float, both from wave heave and by splashing. The two ARGs, A-18 and B-434, were mounted on the mooring line in different ways. ARG A-18 was clamped tightly onto a metal bar, shackled into the mooring line. ARG B-434 was clamped onto the mooring line but mounted in a rubberized harness. They were placed at 20 and 22 m below the surface, respectively. Because the two instruments were nearly collocated, one would expect the two instruments to record the same noise levels unless the mooring line itself generates internal (not water borne) noise. Figure

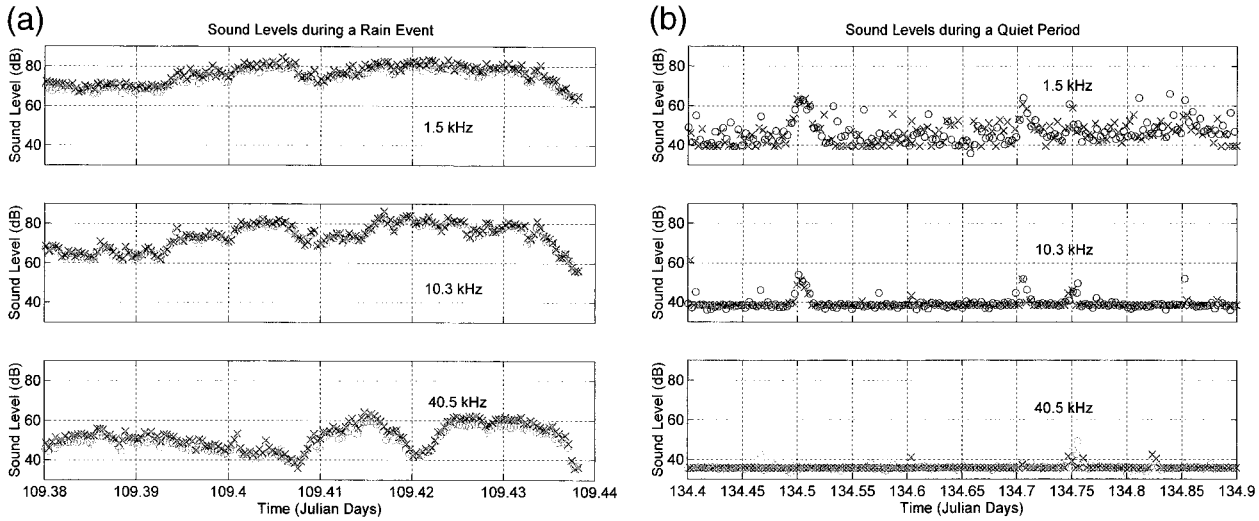

FIG. 3. Sound levels recorded by the ARG-A18 (○) and the ARG-B434 (×) during a loud rain event on (a) yearday 109 and during a quiet period on (b) yearday 134. During the loud event the two ARGs show close agreement. During the quiet period the intermittency of the sound results in more variability at low frequency.

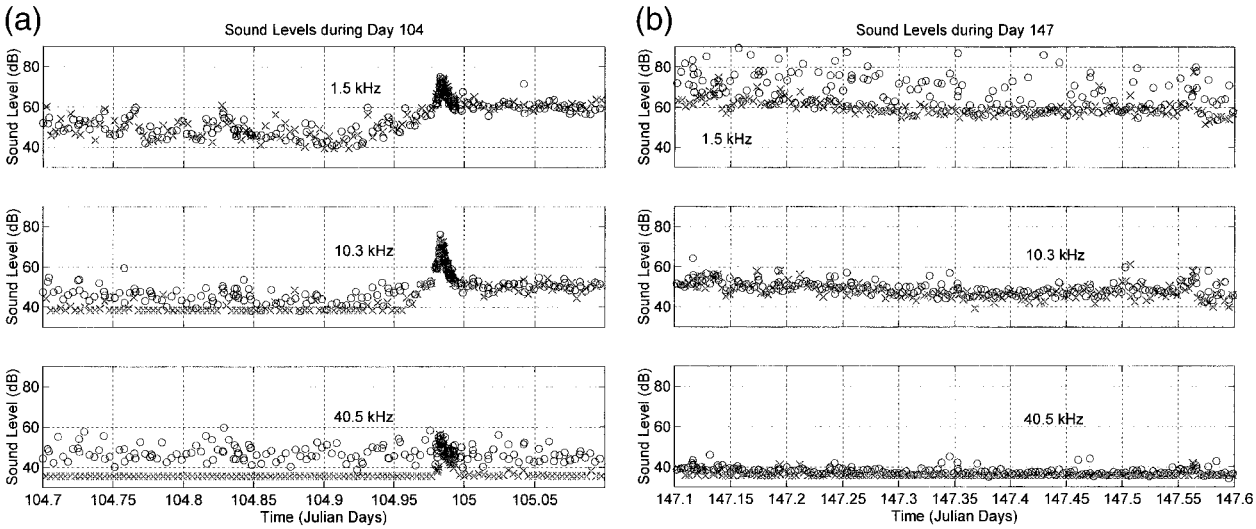

FIG. 4. Sound levels recorded by the ARGs during times of anomalous internal mooring noise. (a) On yearday 104, the hard-mounted ARG-A18 recorded higher sound levels at high frequency, over 10 kHz. (b) On yearday 147, ARG-A18 recorded higher intermittent sound levels at low frequency, under 5 kHz. ARG A-18 (○), ARG B-434 (×).

3 shows the recorded sound levels for a few selected frequencies during a loud underwater event, a rain event on yearday 109 (19 April), and during a quiet period on yearday 134 (14 May). During periods of high ambient sound, in particular, during rain events, the two ARGs did report the same sound levels. In general, this statement was also true during quiet periods, although the variability of the sound levels, especially at low frequencies, is greater. Because the two instruments were not recording the sound at exactly the same time, this variability should be expected. During periods of relative quiet, any sound that might occur, for example, an isolated small splash, will be relatively intermittent, resulting in a relatively high variability in sound level. In contrast, during periods of high sound levels, for example, a heavy rain, the sound sources are more uniformly distributed over the surface and much more continuous temporally. Thus, the variability of the sound field is less, as shown in Fig. 3.

However, there were long periods, lasting days, when there were clear differences in the background noise levels reported by the two instruments. During two periods in the deployment, ARG A-18 recorded intermittent high-frequency noise not detected by ARG B-434. The first period was for several hours immediately after deployment on April 7. The second interval was between yeardays 101 and 108 (11–18 April; Fig. 4a). This noise appears to be tonal ''pings,'' isolated in frequency and time but persistent. This noise is not detected by ARG B-434, in the water just 2 m away but decoupled from the mooring line, suggesting that it is internal mooring line noise. Its exact explanation is unknown.

At other times (Fig. 4b), low-frequency ''bangs'' were recorded by ARG A-18. Again, this noise is isolated in frequency and time but could be persistent. Because mechanical noise, for example, a bang on the buoy float, has low-frequency noise components, extra low frequency noise coupled through the mooring line to the hydrophone was expected. Note that the higher frequencies, over 10 kHz, are not affected by the noise at low frequency. This fact is important for acoustical rainfall analysis, because the signal from rain is mostly contained in the higher frequencies. However, once again this low-frequency noise may be internal to the mooring line, because ARG B434, just 2 m away, does not record it. These conditions, extra low frequency noise in the ARG A-18 data, were most prevalent during the second half of the deployment.

Because of the generally higher noise levels recorded by ARG A-18 and the periods of unusual noise, the subsequent acoustical analysis presented in this paper will concentrate on the data recorded by ARG B-434. Clearly, attention to decoupling the hydrophone from the mooring line is an important consideration on future deployments. However, during rain events, both ARGs recorded the same sound levels, and data from either ARG are valid.

c. Acoustic weather classification

Acoustic analysis of the underwater sound consists of two general steps. First, using the spectral characteristics of the sound, the source is identified. Second, the geophysical quantity of interest is then quantified. The first step, acoustic weather classification, depends on distinctive spectral shapes for different geophysical or anthropogenic noise sources. Some examples of the sound generated by geophysical sources are shown in Fig. 5. The spectral shape of wind-generated sound is

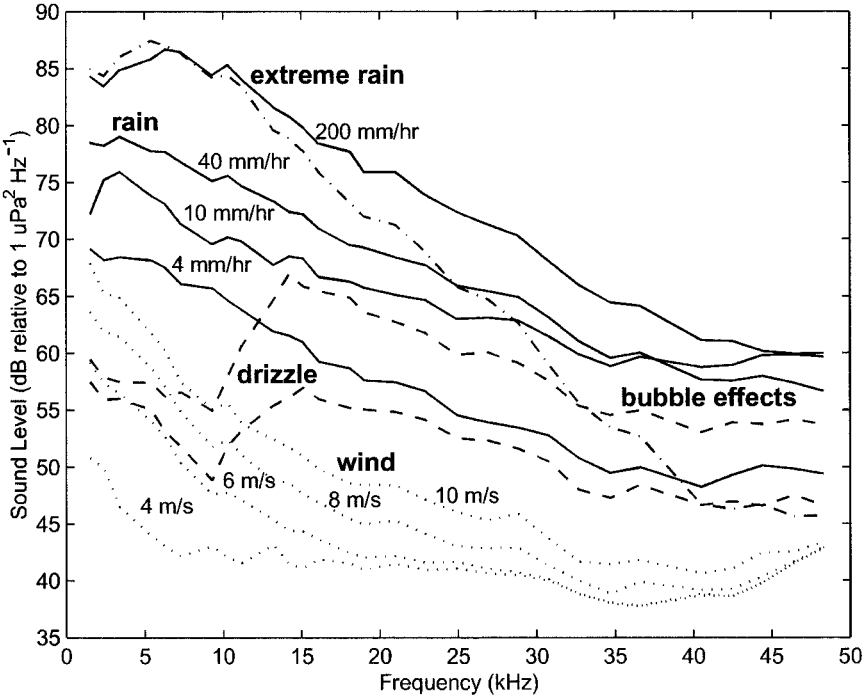

FIG. 5. Samples of geophysical spectra recorded during SCSMEX. Periods of wind only (dotted line), drizzle (dashed line), rain (solid line), and extreme rain (top solid line) are shown. Five min after the start of the extreme rain shown here (yearday 109.42) the sound levels above 20 kHz became depressed to much lower values (dash–dot line). This behavior is an indication of bubble layer formation by the extreme rainfall.

well described (Knudsen et al. 1948; Wenz 1962; and others) and is attributed to breaking wind waves (Farmer and Vagle 1988; Medwin and Beaky 1989). Its characteristic is a relatively uniform negative spectral slope from a peak near 500 Hz to over 25 kHz. Deviations caused by acoustic absorption by ambient bubbles are observed at the higher frequencies (Farmer and Lemon 1984), over 10 kHz, in sea-state conditions with high levels of wave breaking, that is, wind speed over 10 m s^{-1}.

Precipitation has two characteristic spectral features. The first is that light rain or drizzle often contains only small drops, and so the characteristic sound of drizzle is a broad peak in the sound spectrum between 13 and 25 kHz. This signal is known to be sensitive to wind speed (Medwin et al. 1990; Nystuen 1993) and, in fact, has not been detected in oceanic situations when the wind speed is over 8–10 m s^{-1}.

Another sound source from precipitation is due to larger drops, over 2 mm in diameter. The spectral signature of these drops is a broadband (2–50 kHz), relatively flat spectrum (Medwin et al. 1992; Nystuen 1996). This signal dominates the underwater sound field when these drops are present and produces the characteristic sound of heavy rain. Both the sound of drizzle and the sound of heavy rainfall have excess high-frequency (15–30 kHz)-to-low-frequency (2–10 kHz) sound levels relative to wind-only conditions. Furthermore, the sound levels during precipitation are also extremely high relative to wind-only conditions. These signatures allow acoustic classification of wind and rain (Nystuen and Selsor 1997).

One other geophysical feature of the sound spectrum is associated with the extreme weather conditions in which a layer of near-surface ambient bubbles is injected into the ocean. This layer of bubbles absorbs the higher-frequency sound, especially above 10 kHz, causing the high-frequency (10–40 kHz) spectral slope to become very steep. This phenomenon was observed during extreme rainfall events, with rainfall rates over 100 mm h^{-1}, in the SCSMEX data. An example is shown in Fig. 5. Five min after the start of an extreme rainfall event, with a rainfall rate equal to 200 mm h^{-1}, the sound level at 40 kHz had dropped 15 dB relative to the start of the downpour. This is an indication that an ambient bubble layer had formed, suggesting gas injection and turbulent stirring by the heavy rain itself. This phenomenon, an ambient bubble layer formation, has also been detected acoustically for high wind speed conditions (Farmer and Lemon 1984) and during heavy rain with high winds.

Of course, other noises are also present in the ocean, including anthropogenic noises (ships, machinery, mooring lines, etc.) and natural noises (snapping shrimp, other marine life, etc.). Consequently, part of the classification procedure is removal of ''noise.'' Three types of noise were observed in the data. The classic anthro-

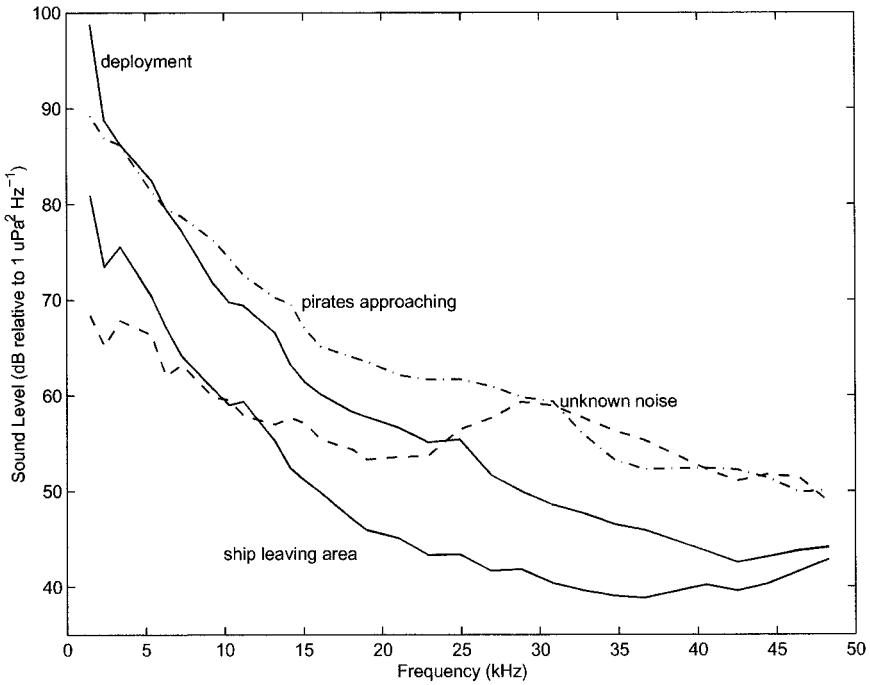

FIG. 6. Other noise sources present in SCSMEX. Shipping has very high levels of low-frequency noise. A mysterious high-frequency noise source was detected. Some spectra showed isolated spikes (tones; not shown).

pogenic noise is ''shipping.'' It is characterized by very high low-frequency sound levels and a 2–10-kHz spectral slope that is steeper than wind-only conditions. This shape is in contrast to the relatively flat sound spectrum from heavy and extreme rainfall between 2 and 8 kHz. Several examples of this shipping noise are present in the SCSMEX data, including initial deployment, mooring recovery, and on 6 May when the mooring was apparently attacked and vandalized (Fig. 6). Shipping noise contaminated 1.95% of the data. A second noise, probably also associated with human activity, was characterized by loud sound levels across the observed frequency spectrum, but especially from 25 to 50 kHz. There was a relative minimum near 20 kHz. This pattern was observed fairly often, in 3.8% of the data, including on the day of the pirate attack when human activity is assumed to be present. The exact physical source of this noise is not known; however, the spectra are not consistent with known geophysical sounds (wind, precipitation, subsurface bubbles) and are thus considered to be noise for the purposes of this study. A final class of noise is spectra containing spikes, that is, loud levels of sound confined to narrow-frequency bands. This kind of noise contamination was present in 1.4% of the data. The source of these ''tones'' is unknown, but may be biological ''chirps'' or anthropogenic bangs. Again, they are not consistent with the geophysical sounds of interest and are thus considered to be noise and are discarded from further analysis. One known biological sound source that interferes with acoustical weather analysis is snapping shrimp. These creatures produce a very loud, broadband sound that often dominates the underwater sound field if present. Fortunately, these shrimp are sessile, living on hard substrata in shallow tropical water, and were not present at the ATLAS mooring site. All together, noise was present in 7.1% of the

TABLE 2. Acoustic classification summary.

	Geophysical sources			Noise sources		
	Wind	Rain	Drizzle	Ships	Spikes	Unknown
No. of records	16 108	2301	1087	409	298	797
Percent of records	76.7%	11.0%	5.2%	1.9%	1.4%	3.8%

Temporal partition of geophysical sound (noise records eliminated)

	Wind	Rain	Drizzle
Minutes	80 038	1371	1499
Percent of time	96.5%	1.65%	1.81%

data. These data were discarded from further analysis. A summary of noise statistics is presented in Table 2.

The data sampling strategy (Nystuen 1998) was designed to provide higher temporal sampling during periods of heavy rainfall. One acoustic measurement is made every 5 min. The spectrum is classified as wind, drizzle, or heavy rain. (Most true noise will also be classified as heavy rain.) The sampling is changed to once every 30 s if heavy rain is detected or once every minute if drizzle is detected, and stays unchanged at once every 5 min if ''wind only'' is detected. Each new spectrum is evaluated, and the sampling interval is changed again, depending on the classification obtained. Thus, the time series of the recorded spectra has a nonconstant time step, depending on changing weather conditions.

d. Ancillary data

Ancillary data include data from the two Doppler radars and the qualitative scientific ship log from the Chinese research ship *Shi Yan 3.* One radar, the NASA TOGA Doppler radar, was deployed on the *Shi Yan 3* and was operated during the IOPs from 5 to 25 May and 4 to 23 June. The second radar was the Bureau of Meteorology Research Centre (BMRC) C-Pol polarimetric C-band Doppler radar (Australia), installed on Dongsha Island. An example of data from the C-Pol radar is shown in Fig. 7. The goal of this paper is to establish rainfall measurements from oceanic surface moorings using the modified R. M. Young rain gauge and the acoustic rain gauges. For this purpose, we only make qualitative comparison with radar data from a single rain event. Full comparison to the radar data is beyond the scope of this paper and is deferred to later analysis.

3. Data analysis

a. Quantifying wind speed

The anemometer height on the ATLAS mooring is 4 m. The data values are 2-min-averaged wind vectors. Using the COARE V2.5b flux algorithm (Fairall et al. 1996) these values are converted to equivalent 10-m-height winds. For these data, the 10-m wind speeds are stronger than the 4-m values by an almost-constant factor of 1.093, that is, wind speeds are 9.3% higher at 10 m.

An algorithm for the acoustic quantification of wind speed is available (Vagle et al. 1990). After sound records containing noise, including precipitation, are removed, the sound level is empirically related to 10-m height wind speed by

$$U_{10} = (10^{\mathrm{SL}_x/20} + 104.3)/53.91, \qquad (1)$$

where SL_8 is the sound level at 8 kHz, and U_{10} is the estimated wind speed at 10 m. This relationship was empirically developed using 8-kHz data from the North Atlantic Ocean (Vagle et al. 1990). It is applied to the SCSMEX acoustic data and is shown in Fig. 8. Also shown in Fig. 8 are wind speed data from the ATLAS surface anemometer (before 6 May), as well as drizzle and rainfall detections. Because of instrument noise, the minimum acoustic wind speed is about 4 m s^{-1}. A comparison of wind speed observations from the buoy anemometer and the ARG is shown in Fig. 9. The variability in the acoustic record is due to a combination of the instantaneous variability in the acoustic record itself (Farmer and Vagle 1988) and to the natural variability of the wind field. The agreement of the acoustic record with the anemometer record is encouraging and is in agreement with expected accuracy (Vagle et al. 1990).

b. Quantifying rainfall rate

Two kinds of acoustic rainfall-rate algorithms are available. Because different raindrop sizes have distinctive acoustic signatures underwater (Medwin et al. 1992), the underwater sound can be decomposed into components associated with each drop size. This decomposition allows an acoustic measure of the drop size distribution in the rain (Nystuen 1996). Once a drop size distribution is obtained, then rainfall rate or equivalent rainfall reflectivity can be calculated. A revised algorithm (Nystuen 1999) is based on over 9000 min of rainfall data collected in a shallow pond in Miami, Florida. Rainfall rates using the inversion will be referred to as R1 in this paper.

A simpler approach is to obtain an empirical relationship that relates the sound level at a given frequency band to rainfall rate, at least for heavy rain (Nystuen et al. 1993). The appropriate frequency band to use is 4–10 kHz. Heavy rain, containing large raindrops, produces sound in this frequency band. At higher frequencies, in particular at the spectral peak from drizzle, the sound level is often poorly related to total rainfall rate. This result is because sound at these frequencies can be produced solely by small raindrops, which often do not constitute a large water volume, and furthermore the peak is sensitive to wind speed (Nystuen 1993). When applied to the data from SCSMEX, the Nystuen et al. (1993) algorithm produced unrealistic values of rainfall rate. The extreme rainfall conditions present in SCSMEX produced high sound levels not observed in Nystuen et al. (1993), making that algorithm invalid for SCSMEX.

However, using the eight nonzero daily accumulation totals from the R. M. Young rain gauge on the ATLAS mooring, a similar new empirical algorithm is proposed:

$$\log_{10}\mathrm{R2} = (\mathrm{SL}_{4-10} - 57)/13, \qquad (2)$$

where SL_{4-10} is the sound level from 4 to 10 kHz (dB) relative to 1 $\mu\mathrm{Pa}^2$ Hz^{-1}, and R2 is the rainfall rate (mm h^{-1}). If SL_{4-10} is less than 57 dB and drizzle or rain is ''detected,'' then the rainfall rate is assumed to be light and R2 is set to 1 mm h^{-1}. This kind of empirical al-

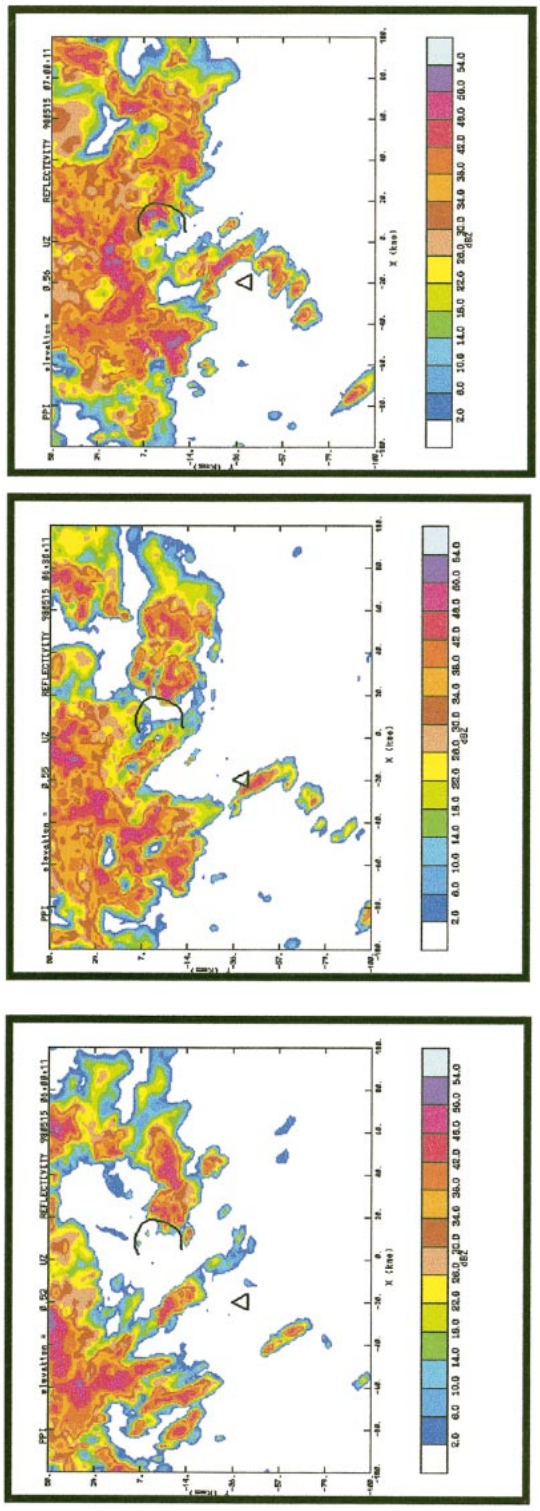

FIG. 7. A sequence of radar images from the BMRC C-Pol Doppler radar located on Dongsha Island. The radar images at 0600, 0630, and 0700 UTC on 15 May show a rain squall passing over the ATLAS buoy location (the triangle symbol) at roughly 0630 UTC. This event was detected by the ARG. Later in the day, the heavy convective rainfall, located to the north in these images, moved over the buoy.

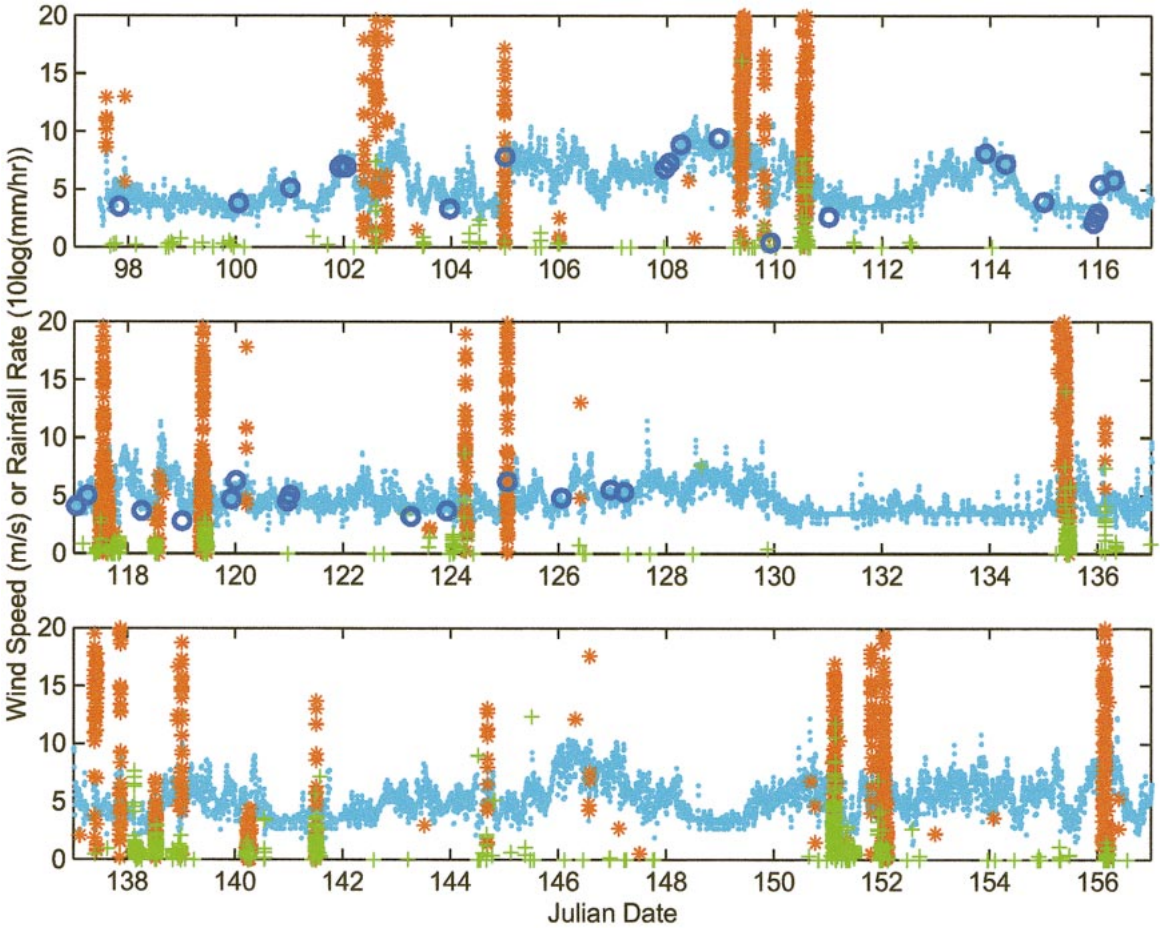

FIG. 8. Acoustic analysis of the sound field during SCSMEX. Acoustic wind speeds (aqua dots) are compared with available ATLAS mooring anemometer data (blue circles). Periods of heavy rain (red *) and drizzle (green +) are indicated. The rainfall rate scale is logarithmic; the plotted values are 10 $\log_{10}(R)$ where R is rainfall rate (mm h^{-1}; for example, 10 is 10 mm h^{-1} and 20 is 100 mm h^{-1}).

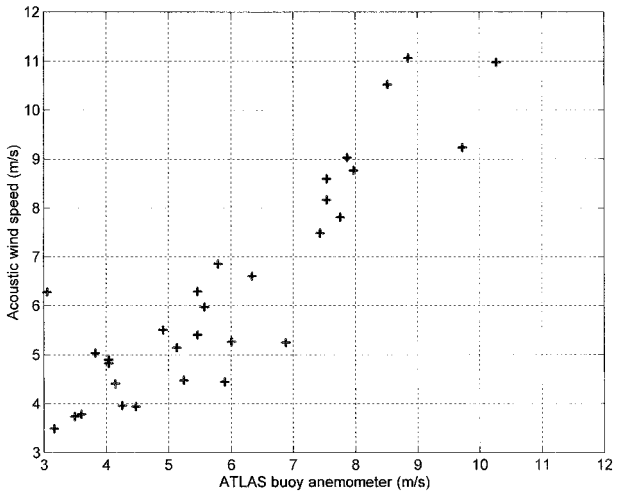

FIG. 9. A comparison of the wind speed measured by the anemometer at 4 m and the ARG estimate of wind speed (36 data points). The acoustic wind speed estimate is only available when it is not raining.

gorithm has been observed to overestimate rainfall during the initial convective part of a storm, when the rain contains a few extraordinarily loud very large raindrops, and then to underestimate rainfall during the stratiform portion of the rain, when the rain contains mostly smaller raindrops (Nystuen et al. 1993).

The surface rainfall data from the R. M. Young rain gauge consisted of the percentage of time raining and the average rainfall rate over a 24-h period. There were eight nonzero values available. The comparison between these data, with the average rainfall rate converted to a daily accumulation, and the acoustic algorithms is given in Table 3. Note that the percentage of time raining each day matches well.

The estimated accumulations are also in relatively good agreement, but there are two days when the R. M. Young gauge reported significantly more rain than the ARG did (yeardays 117 and 118). On these days, light rain occurred over a long period of time. As described earlier, the onboard data-processing strategy used may on occasion cause the R. M. Young gauge to be positively biased.

TABLE 3. A comparison of rainfall accumulation statistics from the R. M. Young rain gauge and the ARGs. The acoustic rainfall accumulation totals are both from ARG-B434. The R1 uses the drop size distribution obtained from the acoustic inversion of the underwater sound and R2 uses Eq. (2).

	R. M. Young gauge		Acoustic rain gauges		
Yearday	Percent time	Accumulation (mm)	Percent time	R1 (mm)	R2 (mm)
103	2%	2	0	0	0
107	0	0	0	0	0
109	13%	110	11%	97	100
110	8%	22	9%	24	19
113	0	0	0	0	0
114	0	0	0	0	0
115	0	0	0	0	0
116	0	0	0	0	0
117	21%	38	25%	17	22
118	3%	7	3%	1	1
119	11%	28	12%	25	22
122	0	0	0	0	0
123	0	0	0	0	0
124	4%	4	5%	6	5
125	2%	11	2%	13	11

A second possible cause for differences in rainfall accumulation may be wind exposure of the ATLAS mooring. On yearday 118, the wind speeds are relatively high. The acoustic inversion was developed using data from a sheltered pond over which wind speeds rarely exceeded 5 m s^{-1}. The estimation of the small-drop population is affected by wind speed (Nystuen 1993, 1997, 1999). In an exposed situation, the small-drop population will be underestimated. In fact, acoustic detection of drizzle (the small-drop signal) has not been observed for wind speed conditions for which wind speed exceeds 8–10 m s^{-1}. In SCSMEX, the acoustic signal from drizzle was weaker than anticipated. Perhaps there was less stratiform rain than expected, or the signal from the small raindrops was being suppressed by the higher local wind conditions. Comparison with the radar data will be important.

Table 4 shows a summary of rainfall events during the deployment. Several events are particularly notable. The detailed acoustic analyses for four of the largest events are shown in Fig. 10. In each case, two high–temporal resolution rainfall-rate estimates (R1 and R2) are available, as is an equivalent reflectivity. Reflectivity is the quantity measured by radars and is estimated acoustically using the acoustically derived drop size distribution. Rainfall classification is also of interest as different rainfall types have different latent heating profiles within the atmosphere. Using the shape of the observed sound spectra (Fig. 5), the data have been partitioned to no-rain, drizzle, and heavy-rain categories (Nystuen and Selsor 1997). Black et al. (1997) attempted to quantify acoustic classification of rainfall by proposing an acoustic discriminant, defined as the ratio of the sound levels in the frequency band 10–30 kHz to the sound level in the frequency band 4–10 kHz. This classification depends on a strong signal from the small raindrops. If these drops produce a loud signal, for example, during drizzle when these drops dominate the drop size distribution, then the ratio of sound levels from 10 to 30 kHz as compared with 4–10 kHz will be relatively positive when compared with times of heavy rainfall when larger drops produce high sound levels across both frequency bands. Given in decibels (no units), the acoustic discriminant is

$$\mathrm{DR} = \mathrm{SPL}_{10\text{–}30\mathrm{kHz}} - \mathrm{SPL}_{4\text{–}10\mathrm{kHz}}, \qquad (3)$$

where SPL_x is the sound intensity (dB) relative to 1 $\mu\mathrm{Pa}^2$ Hz^{-1}, and x is the frequency band, either 10–30 kHz or 4–10 kHz. Note that Black et al. (1997) include a reference to the local noise field within their definition that is inappropriate for the SCSMEX data. The value of DR that is appropriate for the identification of stratiform rain in the SCSMEX data is uncertain but appears to be DR less than -5 dB for convective rain and DR greater than -5 for stratiform rain (Fig. 10). Radar rainfall classification will help to validate these predictions.

The largest single event occurred on yearday 109 (19 April; Fig. 10a). Nearly 100 mm of accumulation is estimated. During the most intense part of this storm, extreme rainfall rates of near 200 mm h^{-1} are observed. At this time, the sound levels above 20 kHz drop sharply over a 5-min period (Fig. 5). This drop suggests the formation of a subsurface bubble layer by the extreme rain. As the rain becomes lighter, the spectral shape distortion quickly vanishes, suggesting that the bubble layer has risen to the surface. The acoustic classification of rainfall is almost entirely convective. Very little ''drizzle'' is detected. The wind speed before and after the event is relatively high (8–10 m s^{-1}) suggesting that the acoustic signal from any stratiform rain associated with this event has been suppressed or, perhaps, that stratiform rain was not present. The value of the acoustic discriminant DR is less than -5 dB throughout the event. This value is much lower than Black et al.'s threshold for convective rain (0 dB) and thus is consistent with their findings. The reflectivity values, over 40 dB*Z*, are also consistent with convective rainfall.

A second interesting event is on yearday 135 (15 May; Fig. 10b). This event is thought to be the start of the monsoon at the buoy location (science log, *Shi Yan 3*). A particularly intense, short-duration rain event occurs at 0630 UTC. This is verified by radar scans (Fig. 7) that show a squall with very high radar reflectivity (over 50 dB*Z*) approaching and moving past the buoy location. Other radar imagery during this day is also consistent with the acoustic analysis. A strong convective rainfall signal is present from yearday 135.37 to 135.42. After yearday 135.42, the rainfall is most likely stratiform. The acoustic discriminant increases at this time but then regains a negative value. The threshold for acoustic classification of convective rainfall is roughly DR less than -5 dB for this event.

This threshold (DR < -5 dB) for the classification

TABLE 4. Data summary for ARG-B434 mounted on the ATLAS rain gauge mooring (PMEL) at 20°22.2′N, 116°31.2′E from 7 Apr–6 Jun 1998 during SCSMEX. Two rainfall accumulations are given for each event: R1 uses the full acoustic inversion and R2 uses Eq. (2). The number of minutes of rain for each event is also given.

		Accumulation			
Yearday	Time (UTC)	R1	R2	Duration	Comments
97 (7 Apr 1998)					Mooring deployment
102 No. 1	0855–0900	1.3	1.1	7 min	Brief convective rain
102 No. 2	1400–1430	9.6	7.9	22 min	Moderate convective rain
102 No. 3	1850–1920	2.0	2.7	23 min	Brief shower, winds 8 m s^{-1}
103 No. 1	0450	0.0	0.1	2 min	Winds drop, rain?
103 No. 2	1120	0.0	0.1	3 min	Drizzle?, noisy spectra
104	2330	2.8	3.0	19 min	Convective rain, winds jump from 4 m s^{-1} to 8 m s^{-1}
109 No. 1	0838–1034	94.2	97.1	120 min	Major event, db*Z* values over 50, no drizzle detection, winds 8–10 m s^{-1}, bubbles present
109 No. 2	1940	2.1	2.0	12.5 min	Brief convective shower, dB*Z* over 40, some drizzle
110	1220–1410	24.1	18.8	112 min	Extreme rainfall at 1355–1410 UTC, winds 5–8 m s^{-1}. The dB*Z* reaches 50, bubbles present
117	1100–1530	16.7	21.8	350 min	Heavy convection from 1240 to 1300 UTC, winds uncertain—Maybe 8–10 m s^{-1}
118	1200 and 1330	0.5	1.0	39.5 min	Two brief showers in fairly high winds
119	0810–1115	25.1	22.2	165 min	Extreme rain, dB*Z* over 50 at 0910–0920 UTC. Winds moderate 6 m s^{-1}, distinct drizzle signal at 1020 UTC.
124 No. 1	0050–0200	0.3	0.7	42 min	Drizzle signal, winds <5 m s^{-1}
124 No. 2	0615	12.8	11.1	31.4 min	Brief heavy convective shower, dB*Z* >40, no drizzle signal
125 (5 May 1998)					Start of IOP No. 1
125	0045–0110	12.8	11.1	31.5 min	Heavy rain, dB*Z* reaches 50, low winds
126	0940–1100				Likely pirate attack, ship approach at 0940 UTC, curious sound spectra 1030–1100 UTC
(15 May = yearday 135) (Monsoon onset)					
135 No. 1	0840–1130 and 0635	43.2	38.6	163 min	Extreme rain squall at 0630 UTC, heavy rain at 0840–1130 UTC, winds are light (4–5 m s^{-1}) with gusts from 8–12 m s^{-1}, dB*Z* exceeds 50
136	0315 and 0810	0.8	0.7	23 min	Two minor events
137 No. 1	0905	12.7	11.4	38 min	Two short convective events
137 No. 2	1010				
137 No. 3	2040–2110	20.8	19.7	27 min	Extreme rainfall rates, winds 10+ m s^{-1}, no sign of drizzle
138 No. 1	0250–0630	1.4	2.1	125 min	Long drizzle signal, winds low, low-reflectivity values
138 No. 2	1210–1300	1.2	1.5	52.5 min	Light convective rain and drizzle, dB*Z* under 40
138 No. 3	2345–0030	5.1	4.8	63 min	Drizzle and squall, ship noise at 2205–2225 UTC
(20 May = yearday 140)					
140 No. 1	450–640	1.3	2.9	115 min	Light rain, winds high
140 No. 2	1300–1400	0.1	0.3	19 min	Drizzle
141 No. 1	1130–1330	1.9	1.9	75 min	Light rain and drizzle
141 No. 2	1730–1800				Strange noise
144	1130–1630	1.0	1.1	23.5 min	Brief showers after fairly high winds, noisy spectra
25 May = yearday 145—End of IOP No. 1					
(31 May 1998 = yearday 151)					
151 No. 1	0200–0400	11.0	6.7	132.5 min	Convective cells in stratiform rain, low winds
151 No. 2	1915–1935	5.4	6.1	16.5 min	Convective rain cell, dB*Z* over 40
152	2345–0300	18.9	14.1	136 min	Brief high rainfall-rate cells followed by light rain, unrealistic rainfall rate at 0100 UTC, dB*Z* over 50, winds 8–10 m s^{-1} (relatively high)
4 Jun = yearday 155—Start of IOP No. 2					
(5 Jun = yearday 156)					
156	0215–0500	20.1	21.9	147.5 min	Two convective cells followed by drizzle, dB*Z* over 50 during second cell at 0315 UTC, winds 8–10 m s^{-1}
157	0400–0600				Recovery of mooring

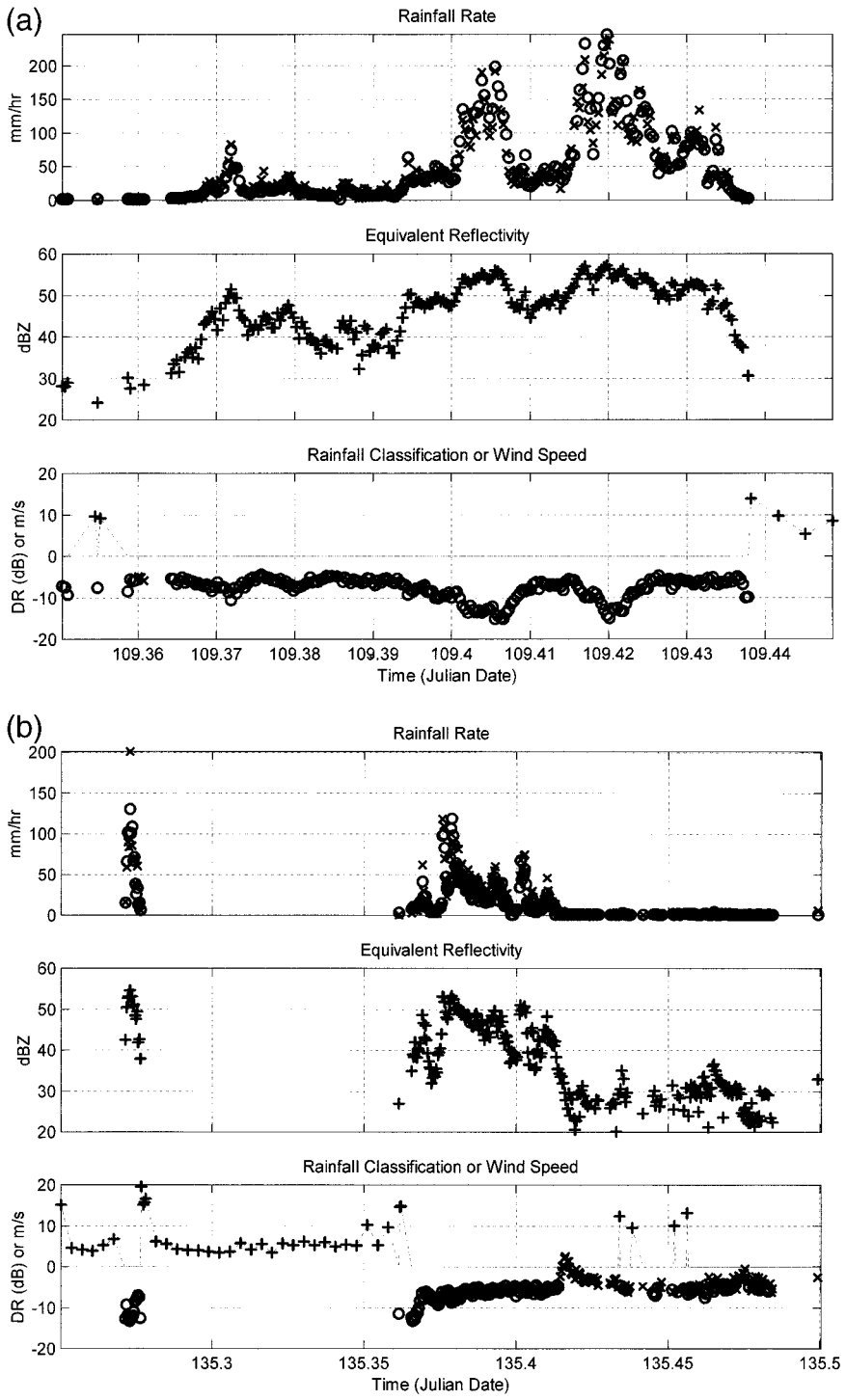

FIG. 10. Detailed acoustic analyses of individual rain events. For each event, two acoustic rainfall-rate estimates are presented, R1 (×) and R2 (○), from the inversion rainfall rate and Eq. (2), respectively (top). The equivalent reflectivity also is shown (middle). The numerical value of the acoustic discriminant DR is shown (bottom) using two different symbols (○ for heavy rain, × for drizzle), where the rainfall-type classification is based on an objective analysis of the shape of the observed sound spectrum. When it is not raining, the numerical value of the acoustic wind speed (m s^{-1}) is shown using a + symbol. (a) A convective rainfall event on yearday 109 (19 Apr). This event had an accumulation of roughly 100 mm. It is also depicted in Fig. 5. Bubble cloud formation associated with extreme rainfall rates occurs at yeardays 109.405 and 109.42. (b) The monsoon onset at the buoy location on yearday 135 (15 May). A strong squall line passed

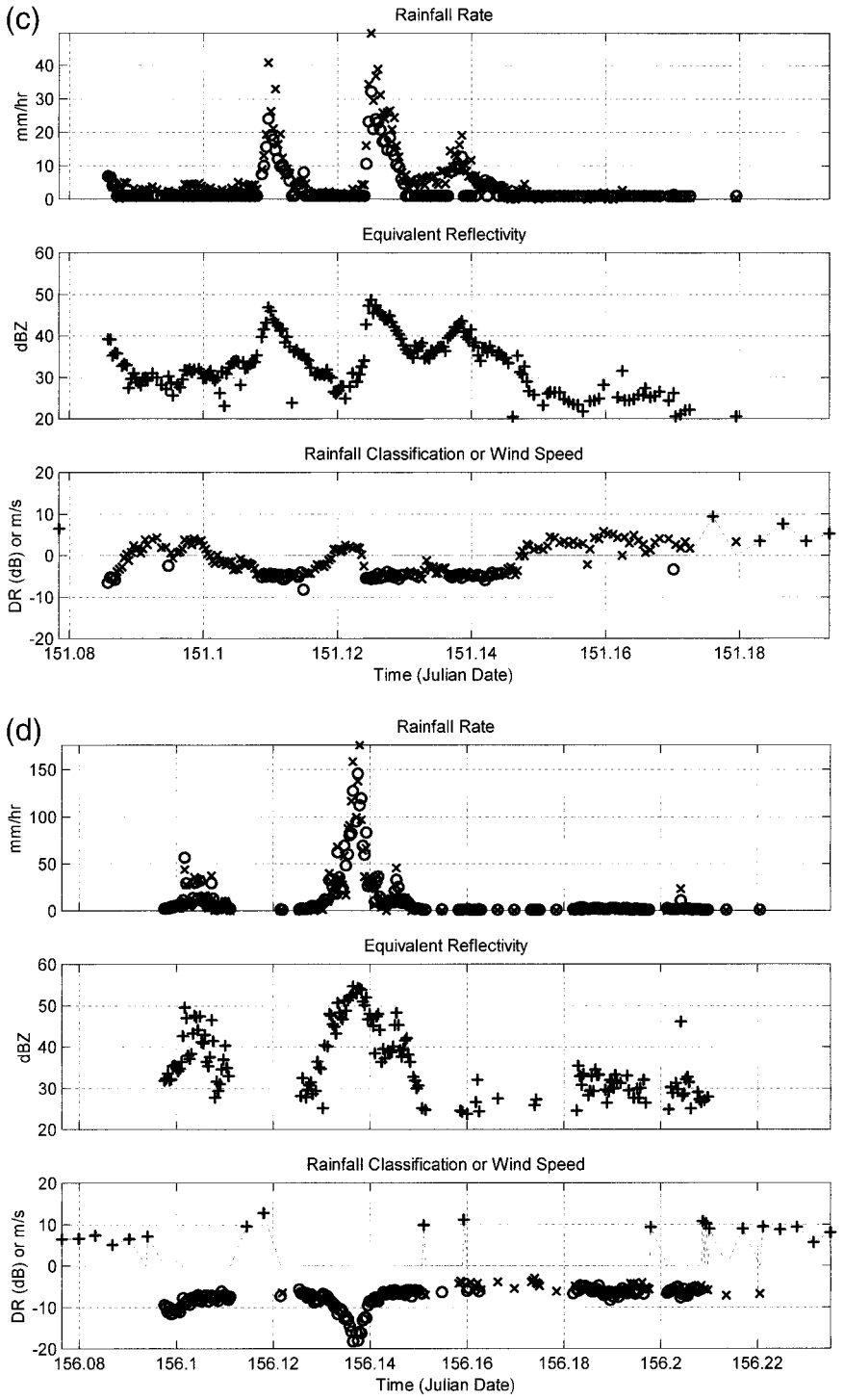

FIG. 10 (*Continued*) over the buoy location at yearday 135.27 (0630 UTC). This squall line is shown in Fig. 7. The magnitude is over 50 dBZ. The main rainfall occurs from yeardays 135.37 to 135.42. At yearday 135.42, the acoustic discriminant becomes relatively positive, indicating a probable change from convective to stratiform rainfall. There is noise at yearday 135.5. (c) A rainfall event on yearday 151 (31 May). Three heavy rain cells are imbedded in light rainfall. There is a strong drizzle signal in the underwater sound field, and the acoustic discriminant is positive. Although this event occurred between the two IOPs, the C-Pol radar on DongSha Island recorded data consistent with the acoustic data. (d) An extreme rainfall event on yearday 156 (5 Jun). The extremely heavy rainfall at yearday 156.35 has large negative values for the acoustic discriminant, suggesting that the discriminant can be used to detect subsurface ambient bubble clouds.

of convective rainfall is also suggested on yearday 151 (31 May; Fig. 10c). Here, three convective rain cells are detected within a longer period of light rain. In this case, the drizzle signal is very apparent in the acoustic record, causing DR to obtain large positive values. On yearday 156 (5 June; Fig. 10d), a very heavy rainfall event is again imbedded in lighter rain. In this case, DR attains very large negative values (−20 dB). The sound field shows very low high-frequency values (above 30 kHz), indicating that an ambient bubble layer has formed. Large negative values of the discriminant (DR < -10 dB) were also observed during the extreme rainfall rates associated with yearday 109 (Fig. 10a), suggesting that the discriminant can also be used to detect the formation of subsurface ambient bubble layers. These data suggest a threshold of roughly DR less than −10 for the detection of subsurface bubbles.

4. Conclusions

Surface rainfall data from the ATLAS ocean surface mooring deployed during SCSMEX are reported using a modified R. M. Young Company rain gauge and two acoustic rain gauges. The R. M. Young rain gauge is part of a new instrumentation package for the ATLAS ocean moorings (Milburn et al. 1996). Data are internally recorded and transmitted to shore in real time via Service Argos. Because of vandalism, only limited data from the Argos satellite link were available from the surface instrumentation. The rainfall data included daily values of percentage of time raining and mean rainfall rate.

The ARGs were mounted underwater at 20- and 22-m depths on the mooring line. One was tightly clamped onto the mooring line; the other was mounted into a rubberized harness. The ARG that was tightly clamped onto the mooring line recorded higher noise levels, especially short duration tones below 1 kHz and from 20 to 50 kHz during several discrete periods during the deployment. This noise may be internal to the mooring line, because the second ARG, in the water just 2 m away, did not detect this noise. Although this noise interfered with wind speed measurements during relatively quiet time periods, it did not interfere with acoustic rainfall measurements, because the signal from the rain is very loud. In fact, during periods of high ambient sound, both ARGs recorded the same signal. Nevertheless, future deployments of ARGs on moorings should use a harness that decouples the hydrophone from the mooring line.

Acoustic weather classification (Nystuen and Selsor 1997) was used to isolate periods of noise, wind, drizzle, and heavy rain and to detect subsurface bubbles. The noise included low-frequency-dominated shipping, an unknown broadband sound with a relative minimum at 20–25 kHz, and spectra that had tonal ''spikes.'' Although these noises are not entirely understood, they represent acoustic spectra that are inconsistent with known geophysical sound sources, for example, breaking waves and precipitation. This noise represented 7.1% of the data and was discarded from further analysis. When it is not raining, acoustic estimates of wind speed are available. These compare well with the available anemometer data.

A variety of rainfall conditions were encountered during SCSMEX. The agreement of daily percentage of time raining between the R. M. Young rain gauge and the ARGs is very good. Two different kinds of acoustic algorithms are used to quantify rainfall rate and also show reasonable agreement with the R. M. Young rain gauge accumulations. The rainfall events were often of short duration with extremely heavy rainfall rates, over 100 mm h^{-1}, and sometimes over 200 mm h^{-1}. These events were easily detected acoustically. Convective rainfall was estimated to occur 1.4% of the time. Relatively little stratiform rain was detected, just 1.3% of the total time. Of course, this record is too short to characterize the climate of the monsoon onset in the South China Sea, but it should be useful for corroboration with other observations in SCSMEX for this season's monsoon onset and will provide a comparison point for future studies.

High–temporal resolution acoustic analyses of several rain events are presented. These events demonstrate the acoustic measurement of equivalent reflectivity, the quantity measured by radar, and the acoustic classification of rainfall type. The acoustic discriminant is relatively more negative than reported by Black et al. (1997) but appears to be able to identify convective and stratiform portions of rain events and may also be able to identify periods of injection of ambient bubble clouds into the ocean surface by extremely heavy rainfall.

Acknowledgments. Funding for the mooring was provided by the Tropical Rainfall Measuring Mission Project Office of NASA. Development of the ARGs for deployment on ocean moorings was sponsored by the Pan American Climate System program in the Office of Global Programs of NOAA. Additional funding is from the National Science Foundation and the Office of Naval Research Ocean Acoustics. We thank Dr. David Tang of National Taiwan University for facilitating the construction, deployment, and recovery of the ATLAS mooring from the R/V *Ocean Researcher*.

REFERENCES

Anderson, S. P., R. A. Weller, and R. B. Lukas, 1996: Surface buoyancy forcing and the mixed layer of the western Pacific warm pool: Observations and 1D model results. *J. Climate*, **9,** 3056–3085.

Barrett, E. C., C. Kidd, and D. Kniveton, 1995: The First Wetnet Precipitation Project (PIP-1): Reflections on the results. *IGARSS'95*, Vol. 1, Firenze, Italy, IEEE International Geoscience and Remote Sensing Society, 649–651.

Black, P. G., J. R. Proni, J. C. Wilkerson, and C. E. Samsury, 1997: Oceanic rainfall detection and classification in tropical and sub-

tropical mesoscale convective systems using underwater acoustic methods. *Mon. Wea. Rev.*, **125,** 2014–2024.

Ebert, E. E., M. J. Manton, P. A. Arkin, R. J. Allam, G. E. Holpin, and A. Gruber, 1996: Results from the GPCP Algorithm Intercomparison Programme. *Bull. Amer. Meteor. Soc.*, **77,** 2875–2887.

Evans, D. L., D. R. Watts, D. Halpern, and S. Bourassa, 1984: Oceanic winds measured from the seafloor. *J. Geophys. Res.*, **89,** 3457–3461.

Fairall, C. W., E. F. Bradley, J. S. Godfrey, G. A. Wick, J. B. Edson, and G. S. Young, 1996: Cool-skin and warm-layer effects on sea surface temperature. *J. Geophys. Res.*, **101,** 1295–1308.

Farmer, D. M., and D. D. Lemon, 1984: The influence of bubbles on the ambient noise in the ocean at high wind speeds. *J. Phys. Oceanogr.*, **14,** 1762–1778.

——, and S. Vagle, 1988: On the determination of breaking surface wave distributions using ambient sound. *J. Geophys. Res.*, **93,** 3591–3600.

Godfrey, J. S., E. F. Bradley, P. A. Coppin, L. F. Pender, T. J. McDougall, E. W. Schulz, and I. Helmond, 1999: Measurements of upper ocean heat and freshwater budgets near a drifting buoy in the equatorial Indian Ocean. *J. Geophys. Res.*, **104,** 13 269–13 302.

Knudsen, V. O., R. S. Alford, and J. W. Emling, 1948: Underwater ambient noise. *J. Mar. Res.*, **7,** 410–429.

Lau, K. M., 1998: The South China Sea Monsoon Experiment (SCSMEX). *Eos, Trans. Amer. Geophys. Union*, **78,** 599, 603.

Lemon, D. D., D. M. Farmer, and D. R. Watts, 1984: Acoustic measurements of wind speed and precipitation over a continental shelf. *J. Geophys. Res.*, **89,** 3462–3472.

McPhaden, M. J., and Coauthors, 1998: The Tropical Ocean–Global Atmosphere (TOGA) observing system: A decade of progress. *J. Geophys. Res.*, **103,** 14 169–14 240.

Medwin, H., and M. M. Beaky, 1989: Bubble sources of the Knudsen sea noise spectrum. *J. Acoust. Soc. Amer.*, **83,** 1124–1130.

——, A. Kurgan, and J. A. Nystuen, 1990: Impact and bubble sound from raindrops at normal and oblique incidence. *J. Acoust. Soc. Amer.*, **88,** 413–418.

——, J. A. Nystuen, P. W. Jacobus, D. E. Snyder, and L. H. Ostwald, 1992: The anatomy of underwater rain noise. *J. Acoust. Soc. Amer.*, **92,** 1613–1623.

Milburn, H. B., P. D. McLain, and C. Meinig, 1996: ATLAS buoy—Reengineered for the next decade. *Proc. IEEE Oceans '96*, Fort Lauderdale, FL, Institute of Electrical and Electronics Engineers, 698–702.

Nystuen, J. A., 1993: An explanation of the sound generated by light rain in the presence of wind. *Natural Physical Sources of Underwater Sound*, B. R. Kerman, Ed., Kluwer Academic, 659–668.

——, 1996: Acoustical rainfall analysis: Rainfall drop size distribution using the underwater sound field. *J. Acoust. Soc. Amer.*, **13,** 74–84.

——, 1997: Quantitative rainfall measurements using underwater sound. *Natural Physical Processes Associated with Sea Surface Sound*, T. Leighton, Ed., University of Southampton, 73–82.

——, 1998: Temporal sampling requirements for autonomous rain gauges. *J. Atmos. Oceanic Technol.*, **15,** 1254–1261.

——, 1999: Performance of automatic rain gauges under different rainfall conditions. *J. Atmos. Oceanic Technol.*, **16,** 1025–1043.

——, and H. D. Selsor, 1997: Weather classification using passive acoustic drifters. *J. Atmos. Oceanic Technol.*, **14,** 656–666.

——, C. C. McGlothin, and M. S. Cook, 1993: The underwater sound generated by heavy precipitation. *J. Acoust. Soc. Amer.*, **93,** 3169–3177.

Shaw, P. T., D. R. Watts, and H. T. Rossby, 1978: On the estimation of oceanic wind speed and stress from ambient noise measurements. *Deep-Sea Res.*, **25,** 1225–1233.

Vagle, S., W. G. Large, and D. M. Farmer, 1990: An evaluation of the WOTAN technique for inferring oceanic wind from underwater sound. *J. Atmos. Oceanic Technol.*, **7,** 576–595.

Wenz, G. M., 1962: Acoustic ambient noise in the oceans: Spectra and sources. *J. Acoust. Soc. Amer.*, **34,** 1936–1956.